Peng *et al.*
Chinese Journal of Mechanical Engineering (2022) 35:23
https://doi.org/10.1186/s10033-022-00692-6

Chinese Journal of Mechanical Engineering

ORIGINAL ARTICLE

Open Access

Transfer Path Contribution to Floor Vibration of Metro Vehicles Based on Operational Transfer Path Analysis Method

Laixian Peng[1], Jian Han[1], Jiaxing Nie[2], Xinbiao Xiao[3*] and Caiying Mi[1]

Abstract

Operational transfer path analysis (OTPA) is an advanced vibration and noise transfer path identification and contribution evaluation method. However, the application of OTPA to rail transit vehicles considers only the excitation amplitude and ignores the influence of the excitation phase. This study considers the influence of the excitation amplitude and phase, and analyzes the contribution of the secondary suspension path to the floor vibration when the metro vehicle runs at 60 km/h, using an analysis based on the OTPA method. The results show that the vertical direction of the anti-rolling torsion bar area provides the maximum contribution to the floor vibration, with a contribution of 22.1%, followed by the longitudinal vibration of the air spring area, with a contribution of 17.1%. Based on the contribution analysis, a transfer path optimization scheme is proposed, which may provide a reference for the optimization of the transfer path of metro vehicles in the future.

Keywords: OTPA, Secondary suspension, Contribution analysis, Transfer path optimization scheme, Metro vehicles

1 Introduction

In recent years, metro trains have become an indispensable part of urban public transportation in China. With the rapid development of metro cars, new challenges have emerged, necessitating further research. Noise control is one of the key issues in improving the ride comfort of metro trains. Determining the excitation source and its transfer path is an important prerequisite for noise control.

When the train is running at a speed of 30–80 km/h, wheel-rail rolling contact becomes the main source of excitation [[1], [2]]. Fan et al. [[3]] found that the major source of the interior noise in train cars is the structural-borne sound radiated by floor vibration. Zhang et al. [[4]] found that the bogie area noise and sound source at the middle of the coach contribute significantly to the interior noise. The most direct and effective method of noise control is the elimination of the excitation source. Furthermore, it is important to identify the transfer path of the main source of excitation.

The transfer path analysis (TPA) method [[5]–[8]] is an effective method to obtain the contribution of each transfer path. However, it takes a lot of effort and time to obtain all the transfer functions. Operational transfer path analysis (OTPA) is an advanced vibration and noise transfer path identification and contribution evaluation method [[9]]. Klerk et al. [[10]] elaborated on the theory, modeling principles, and precautions of the OTPA method and applied the OTPA method to practical engineering. De Sitter [[11]] applied OTPA to study the noise, vibration, and harshness (NVH) problems of a car, and the results showed that no disassembly was required for the analysis and operational forces did not have to be eliminated. Keizer et al. [[12]] used the OTPA method to analyze the contribution of the noise sources of a ship, such as engines, gearboxes, and propellers. Robert [[13]] applied OTPA to study the vibration and noise problems

*Correspondence: xinbiaoxiao@163.com
[3] State Key Laboratory of Traction Power, Southwest Jiaotong University, Chengdu 610031, China
Full list of author information is available at the end of the article

of a high-speed train bogie, and found that OTPA was faster and often cheaper than traditional TPA. However, when OTPA is applied to complex mechanical systems, there is a problem of crosstalk between vibration sources [[14]]. Putner et al. [[15]] pointed out that the reference points of the excitation source should be as close as possible to the excitation source to reduce the effect of crosstalk. Mihkel [[16]] applied singular value decomposition (SVD) and principal component analysis (PCA) to solve the crosstalk problem of OTPA, which canceled crosstalk by truncating small singular values or principal components. Cheng et al. [[17]] proposed a novel crosstalk cancelation method based on independent component analysis (ICA) to eliminate crosstalk effects between the reference signals of OTPA. Zhang [[18]] performed crosstalk cancelation pre-processing on experimental data to achieve more accurate data for the TPA, and the experiment proved that the method can obtain more accurate contribution results for each path. Lei [[19]] used the OTPA method to analyze the transfer paths of metro vehicle interior noise and found that the major path among the structural excitation paths is the vertical damper on both sides of the bogie.

In summary, the OTPA method has been progressively applied in the field of rail transit vehicles to analyze the contribution of the transfer path. However, in previous studies, the application of OTPA in rail transit vehicles has ignored the influence of the excitation phase. Based on the results of sound source identification, this study found that when the metro vehicle was running on the roadbed at a speed of 60 km/h, the main sound source of the interior noise was located in the floor area above the bogie. Furthermore, the vibration and sound radiation of the floor area above the bogie dominated the interior noise level. There are two excitation sources for floor vibration and sound radiation. One is the structural excitation caused by the wheel-rail interaction, and the other is the noise excitation in the bogie area. Combined with the vibration test results, it was found that the vertical vibration of the floor was significantly higher than the horizontal and vertical vibrations, and the vertical vibration of the floor radiated noise more easily. Therefore, based on the OTPA method, this study considers the influence of the excitation amplitude and phase, takes the floor vertical vibration as the target point, and analyzes the contribution of the secondary suspension path to the floor vibration. At the same time, based on the results of the contribution analysis, a scheme of transfer path optimization is presented. A research sketch is presented in Figure 1.

2 OTPA Method Theory

This section introduces the main theories of OTPA and provides a theoretical basis for the subsequent contribution analysis experiments. OTPA is a signal processing method that uses numerical calculation to obtain the transfer functions between the input and output signals to obtain the contributions of the excitation sources or transfer paths to the target point response [[11], [21], [22]].

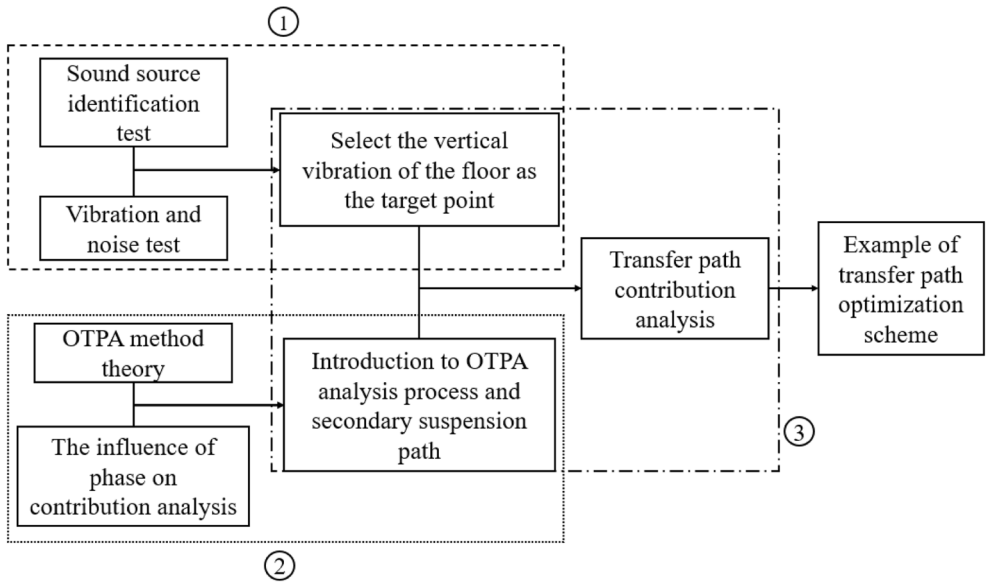

Figure 1 Research sketch

The OTPA method theory is based on the linearized and time-invariant system. The input and output of the system can be expressed as

$$\boldsymbol{Y}(j\omega) = \boldsymbol{X}(j\omega)\boldsymbol{H}(j\omega), \tag{1}$$

where $\boldsymbol{Y}(j\omega)$ is the output vector of the response points and $\boldsymbol{X}(j\omega)$ is the input vector of the reference points, $\boldsymbol{H}(j\omega)$ is the transfer functions matrix.

For the general vibration and noise measurements, the collected signals are usually vibration acceleration signals and sound pressure signals. According to the equation $\boldsymbol{H}(j\omega) = \boldsymbol{X}(j\omega)^{-1}\boldsymbol{Y}(j\omega)$, the transfer functions matrix can be obtained as follows.

$$\begin{pmatrix} H_{a1} \\ \vdots \\ H_{an} \\ H_{s1} \\ \vdots \\ H_{sm} \end{pmatrix} = \begin{pmatrix} a_{11} & \cdots & a_{1n} & s_{11} & \cdots & s_{1m} \\ a_{21} & \cdots & a_{2n} & s_{21} & \cdots & s_{2m} \\ a_{31} & \cdots & a_{3n} & s_{31} & \cdots & s_{3m} \\ a_{41} & \cdots & a_{4n} & s_{41} & \cdots & s_{4m} \\ \vdots & \ddots & \vdots & \vdots & \ddots & \vdots \\ a_{k1} & \cdots & a_{kn} & s_{k1} & \cdots & s_{km} \end{pmatrix}^{-1} \begin{pmatrix} Y_1 \\ Y_2 \\ Y_3 \\ Y_4 \\ \vdots \\ Y_k \end{pmatrix}, \tag{2}$$

where k is the number of operating conditions, n, m respectively represents the number of vibration reference points and acoustic reference points, and there is a necessary condition is $k>m+n$. However, the equation is solved directly, numerical problems will appear and the wrong transfer functions matrix may be obtained. Therefore, there is needed to solve the problem of solving the equation by singular value decomposition (SVD).

The reference points matrix $\boldsymbol{X}$ can be expressed as

$$\boldsymbol{X} = \boldsymbol{U}\boldsymbol{S}\boldsymbol{V}^{\mathrm{T}}, \tag{3}$$

where $\boldsymbol{U}$ is a $k \times k$ matrix,$\boldsymbol{U}\boldsymbol{U}^{\mathrm{T}} = \boldsymbol{I}$, $\boldsymbol{V}$ represents a $(m+n) \times (m+n)$ matrix, $\boldsymbol{V}\boldsymbol{V}^{\mathrm{T}}=\boldsymbol{I}$. $\boldsymbol{S}$ is a $k \times (m+n)$ matrix and $\boldsymbol{S} = \begin{bmatrix} \boldsymbol{Z} & 0 \\ 0 & 0 \end{bmatrix}$, here $\boldsymbol{Z} = \mathrm{diag}(\sigma_1 \cdots \sigma_r)$.

At this moment, the matrix has been decoupled by SVD and a part of the noise interference is removed by the principal component analysis (PCA) method. Thereby the accuracy of the transfer functions matrix is improved. However, eigenvalue decomposition only applies to square matrices, so mathematical transformation are required when performing SVD:

$$\boldsymbol{X}^{\mathrm{T}}\boldsymbol{X}=\boldsymbol{V}\boldsymbol{S}^{\mathrm{T}}\boldsymbol{U}^{\mathrm{T}}\boldsymbol{U}\boldsymbol{S}\boldsymbol{V}^{\mathrm{T}} = \boldsymbol{V}(\boldsymbol{S}^{\mathrm{T}}\boldsymbol{S})\boldsymbol{V}^{\mathrm{T}}, \tag{4}$$

$$\boldsymbol{X}\boldsymbol{X}^{\mathrm{T}} = \boldsymbol{U}\boldsymbol{S}\boldsymbol{V}^{\mathrm{T}}\boldsymbol{V}\boldsymbol{S}^{\mathrm{T}}\boldsymbol{U}^{\mathrm{T}} = \boldsymbol{U}(\boldsymbol{S}\boldsymbol{S}^{\mathrm{T}})\boldsymbol{U}^{\mathrm{T}}, \tag{5}$$

The eigenvalues of matrix $\boldsymbol{X}\boldsymbol{X}^{\mathrm{T}}$ and $\boldsymbol{X}^{\mathrm{T}}\boldsymbol{X}$ are equal to the square of the singular value matrix $\boldsymbol{X}$. The column vector of the matrix $\boldsymbol{V}$ is the eigenvector of the matrix $\boldsymbol{X}^{\mathrm{T}}\boldsymbol{X}$, and the row vector of the matrix $\boldsymbol{U}$ is the eigenvector of matrix $\boldsymbol{X}\boldsymbol{X}^{\mathrm{T}}$. According to Eq. (1):

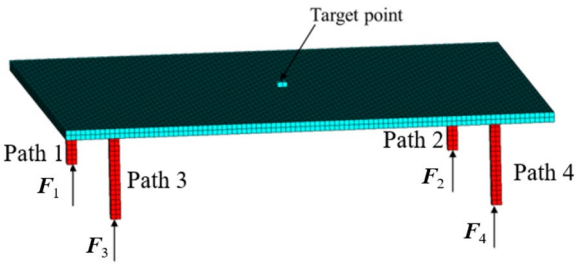

Figure 2 The simplified model

$$\boldsymbol{H} = (\boldsymbol{X}^{\mathrm{T}}\boldsymbol{X})^{-1}\boldsymbol{X}^{\mathrm{T}}\boldsymbol{Y}=\boldsymbol{X}^{+}\boldsymbol{Y}, \tag{6}$$

where $\boldsymbol{X}^{+}$ is the generalized inverse matrix of the input matrix $\boldsymbol{X}$.

$$\boldsymbol{X}^{+}= \boldsymbol{V}\boldsymbol{S}^{-1}\boldsymbol{U}^{\mathrm{T}}. \tag{7}$$

The transfer functions after SVD as follows:

$$\boldsymbol{H}=\boldsymbol{V}\boldsymbol{S}^{-1}\boldsymbol{U}^{\mathrm{T}}\boldsymbol{Y}. \tag{8}$$

The target point response can be synthesized and the contribution of the excitation sources and transfer paths can be calculated by the input signals and Eq. (1) after the transfer functions is obtained.

3 Influence of Phase on Contribution Analysis

This section uses a simplified finite element model to indicate that the contribution analysis should consider the phase of excitation. To determine whether the evaluation method that considers only the excitation amplitude can effectively rank the contributions to the target response of the transfer paths, a simplified model using the finite element method to analyze the contribution of the transfer paths was established in this study. The simplified model is shown in Figure 2.

The simplified model consisted of a steel plate and four identical steel columns. The size of the steel plate was 1000 mm × 1000 mm × 20 mm, and the size of each steel column was 20 mm × 20 mm × 160 mm. The four transfer paths represented by the four steel columns are evenly distributed at the four corners of the rectangle, and the target point is at the geometric center of the four excitation points. The transfer functions from each excitation point to the target point were obtained using the finite element method. Because the simplified model is a symmetric structure, the transfer functions of the four paths are the same. The transfer function of each path is shown in Figure 3.

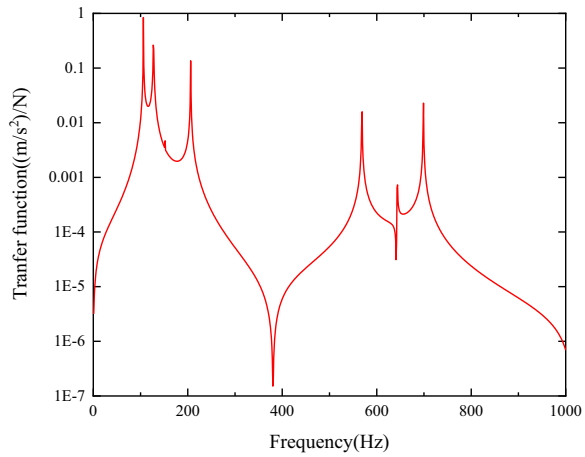

Figure 3 Transfer function of each path

Table 1 Operation 1

Force	Amplitude (N)	Phase (°)	Frequency (Hz)
F_1	50	−180	200
F_2	40	45	200
F_3	40	10	200
F_4	30	−30	200

Table 2 Operation 2

Force	Amplitude (N)	Phase (°)	Frequency (Hz)
F_1	50	45	200
F_2	40	60	200
F_3	40	30	200
F_4	30	−30	200

Two different sets of excitations were added to the bottoms of the four steel columns. The specific information of the excitations is shown in Tables 1 and 2.

The contributions of the four excitations and the target point response can be directly obtained because the excitations and transfer functions are known; the results are shown in Figure 4.

As shown in Figure 4, when excitations of the same amplitude and different phases are applied to the same transfer path, the corresponding contribution of each path to the target point is different. For example, in Operation 1, Path 3 has the largest contribution to the target point, whereas in Operation 2, Path 1 has the largest contribution to the target point. The main reason for the difference in the results is the change in the excitation phase. Hence, it is necessary

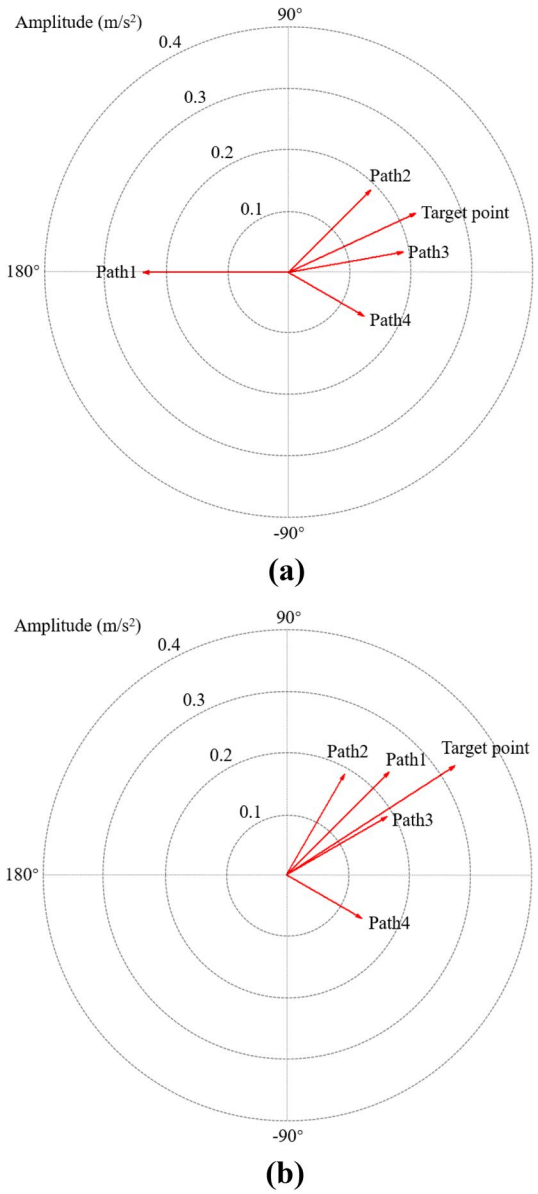

Figure 4 The vector diagram of the transfer paths at 200 Hz for **a** Operation 1 and **b** Operation 2

to comprehensively consider the influence of the amplitude and the phase in the contribution analysis.

In the vector diagram at a certain frequency, if we assume that the phase difference between the x path and the target point is θ_x, and the amplitude of the x path is A_x, then the contribution G_x of the x path to the target point is as follows:

$$G_x = A_x \cos(\theta_x). \tag{9}$$

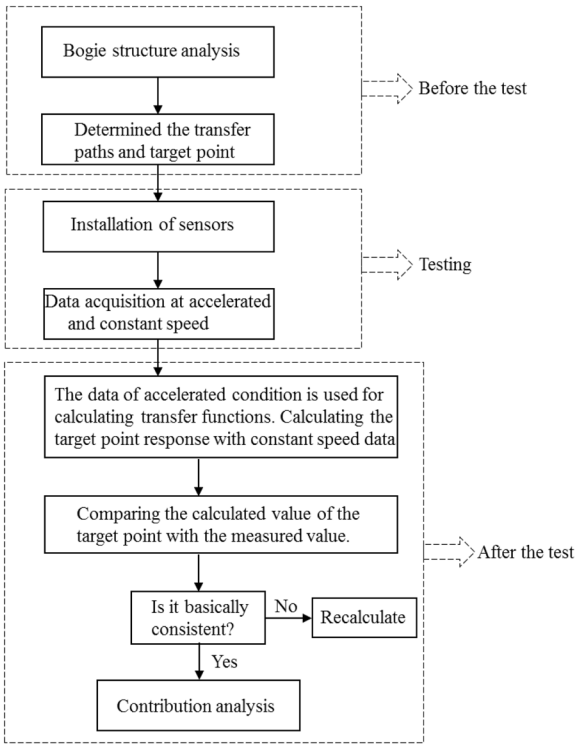

Figure 5 Flow chart of transfer path analysis

The path contributes positively to the target point when G_x is positive, and the path makes a negative contribution to the target point when G_x is negative. Because there is a vector diagram at each frequency, the comprehensive contribution of the transfer path is calculated by summing the contributions G_x in the frequency range of 300–800 Hz.

$$Z_x = \sum_{n=1}^{n} G_x, \tag{10}$$

where n is the number of frequencies and Z_x is the comprehensive contribution of the x path to the target point.

4 Test of OTPA

This section explains the main process of the metro vehicle transfer path contribution analysis, and points out the path considered in the contribution analysis results later. The basic process of the metro vehicle transfer path contribution analysis based on the OTPA method is shown in Figure 5.

Pre-test analysis showed that the excitation of the metro vehicle floor vibration can be divided into two parts: air excitation and structural excitation in the bogie area. The air excitation is noise in the bogie area, and the structural excitation is bogie vibration caused by wheel-rail interactions. There are five secondary suspension components that transmit structural excitation to the floor: the air spring, anti-rolling torsion bar, lateral damper, core plate, and traction bar. They are labeled ① to ⑤, respectively, in Figure 6. In addition, the bogie area noise excitation is represented by ⑥. During the test, the arrangement of the reference points should represent the vibration of the components as much as possible. To prevent crosstalk, the reference points should not be too close. Because the reference point of the core plate and that of the traction rod were too close, and it was difficult to arrange the acceleration sensor in the traction rod area, the core plate path (represented by ④) and traction rod path (represented by ⑤) were merged into one path, the core plate area path (represented by (4)). In summary, the reference points were arranged only at the positions of the anti-rolling torsion bar area, lateral damper area, core plate area, and traction bar area in the test. Considering the horizontal, vertical, and longitudinal directions of the four structural excitation paths and the noise excitation path in the bogie area, a total of 13 transfer paths were considered.

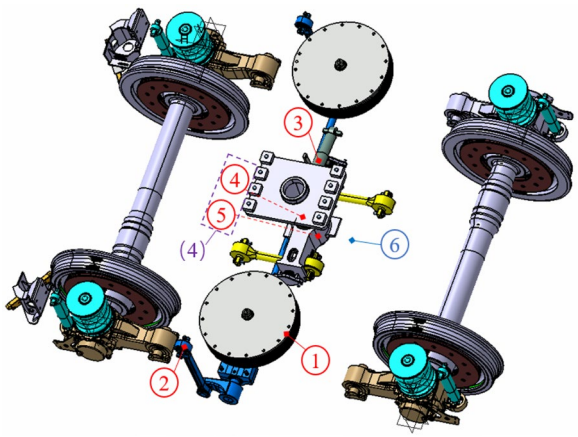

Figure 6 Reference point location diagram

Thus, all transfer paths were as shown in Table 3.

5 Transfer Path Contribution Analysis

Both the amplitude and phase of excitation should be considered in the contribution analysis. Based on the contribution analysis method considering the amplitude and phase, the contributions of secondary suspension transfer paths to the floor vibration were analyzed. In addition, based on the results of the contribution analysis, a transfer path optimization scheme is presented.

Figure 7 shows the noise frequency spectrum of the passenger room sound from 1.6 m to the floor above the bogie area of TC01. The vehicle interior noise energy is

Table 3 Transfer paths

Path number	Transfer path
Path 1	Vertical direction of the air spring area
Path 2	Lateral direction of the air spring area
Path 3	Longitudinal direction of the air spring area
Path 4	Vertical direction of the anti-rolling torsion bar area
Path 5	Lateral direction of the anti-rolling torsion bar area
Path 6	Longitudinal direction of the anti-rolling torsion bar area
Path 7	Vertical direction of the lateral damper area
Path 8	Lateral direction of the lateral damper area
Path 9	Longitudinal direction of the lateral damper area
Path 10	Vertical direction of the core plate area
Path 11	Lateral direction of the core plate area
Path 12	Longitudinal direction of the core plate area
Path 13	Noise at the bogie area

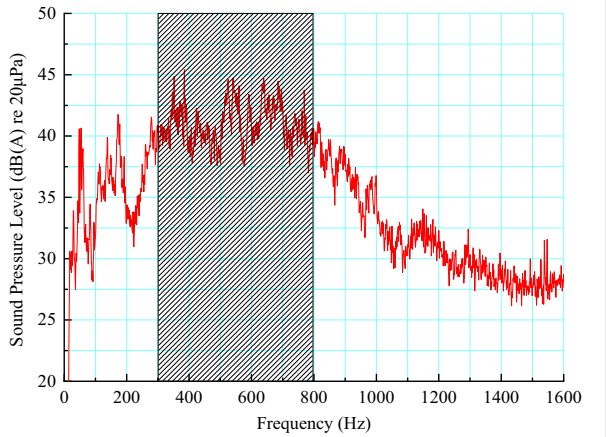

Figure 7 Frequency spectrum of passenger room noise above bogie

mainly concentrated in the frequency range of 300–800 Hz.

Figure 8 shows the sound pressure cloud diagram of the sound source identification test results from the passenger room of TC01 at 315 Hz, 400 Hz, 500 Hz, and 630 Hz when the metro vehicle was running at 60 km/h.

Figure 8 shows that the floor area is the major contributing source to the interior noise in the frequency range of 300–800 Hz. Therefore, the subsequent analysis of the secondary transfer path contributions mainly focuses on the frequency range of 300–800 Hz.

The transfer functions were calculated based on the operational data of the test under accelerated conditions, and the calculated value of the target point was obtained by using the reference point data of another group of typical operational data at 60 km/h. The calculated result was compared with the response of the target point obtained from the actual test, as shown in Figure 9.

Figure 9 shows the frequency spectrum of the target point calculated by the OTPA method and the plot of the measured value versus time. The calculated value was very close to the measured value and can be well matched at each significant peak. This verifies that calculated results are accurate, so they can be used for contribution analysis in the following section.

To understand the contribution level of each transfer path, the general method is to sort the overall value of the transfer path contributions and obtain the most important contribution path. Figure 10 is a histogram of the overall value of the transfer path contributions in the frequency range of 300–800 Hz when the vehicle was running at a constant speed of 60 km/h.

Figure 10 shows that at a constant speed of 60 km/h, the lateral direction of the lateral damper area has the largest transfer path contribution, and the second largest contribution is that of the vertical direction of the lateral damper area. Because the target point response is the superposition of all path contribution vectors and the contributions' overall value is the superposition of the energy, only the amplitude of the transfer path contributions is considered; the influence of the phase is not considered here. The amplitude and phase of the transfer path contributions are considered in the following part, and the contributions of each path are evaluated.

Similarly, the relationship between the transfer paths and target response amplitude and phase in the frequency range of 300–800 Hz is shown in Figure 11. Figure 11(a) shows the amplitude–frequency relationship diagram, in which redder color indicates a larger amplitude. Figure 11(b) shows the phase–frequency relationship diagram, in which the darker color (redder or bluer) indicates a larger phase difference between the paths and the target point. The closer the color is to green, the smaller the phase difference between the paths and the target point.

Figures 10 and 11 show that the contribution amplitudes of the lateral and vertical directions of the lateral damper area (Paths 7 and 8) are larger than those of all other paths, but the phase of each path varies greatly at different frequencies. There is no obvious transfer path with larger amplitude, and the smaller phase difference is found in this frequency band, that is, the path with the largest contribution to the target response cannot be identified in Figure 11. Therefore, in order to understand the transfer paths of large contributions, it is necessary to analyze the contribution of 300–800 Hz considering the amplitude and phase.

The structural excitation contribution and bogie area noise excitation contribution in the frequency range of 300–800 Hz were calculated using Eq. (10). The results showed that the contribution of structural excitation was

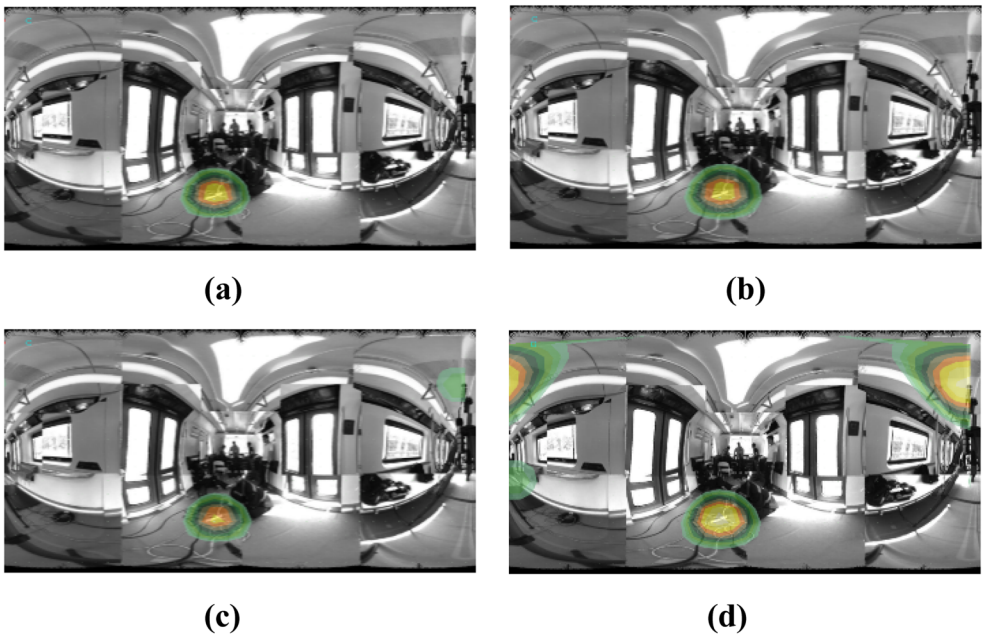

Figure 8 The interior sound source identification results at 60 km/h for **a** 315 Hz, **b** 400 Hz, **c** 500 Hz, and **d** 630 Hz

86.6%, and the contribution of the bogie area noise excitation was 13.4%. The contribution of the bogie area noise excitation was small compared to the structural excitation. Therefore, in the following contribution analysis, the influence of the bogie area noise excitation is ignored. In this case, only the contribution of structural excitation considering amplitude and phase are analyzed in the following. The contributions of the secondary transfer paths were calculated, and the results are shown in Figure 12.

Figure 12 shows that only the longitudinal direction of the lateral damper area makes a negative contribution in the transfer paths of the secondary system, but its influence is small in the frequency range of 300–800 Hz. The vertical direction of the anti-rolling torsion bar area provides the maximum contribution to the floor vibration, followed by the longitudinal direction of the air spring area.

To reduce the target point response, the contribution analysis method considering the overall value (Method A) and the contribution analysis method considering amplitude and phase (Method B) were analyzed. It was assumed that the transfer characteristics of the secondary suspension can be arbitrarily optimized, the amplitude of the transfer path contributions is reduced to a certain extent, and the phase is unchanged. The major transfer paths obtained by the two methods were separately optimized to compare the changes in the target point response.

The lateral and vertical directions of the lateral damper area are the major transfer paths obtained by Method A, and the vertical direction of the anti-rolling torsion bar area and the longitudinal direction of the air spring area are the major transfer paths obtained by Method B. It is assumed that the major paths obtained by Method A and Method B are optimized separately, and the amplitude of the major path contribution is reduced by 20%, 40%, 60%, and 80%, respectively. The overall value of the target point response was obtained and compared with the initial value, as shown in Table 4.

Table 4 shows that there is a significant effect on reduction of the target point response from the optimization of the major paths obtained by Method B, whereas the result of optimization of the major paths from Method A has little effect on the target point response. Therefore, it is more reasonable to use Method B to evaluate the contribution of transfer paths to the target point. It can be found that the target point response is increased when the contribution of the two major paths is reduced to a certain extent. The reason is that the amplitude of the major contribution paths decreases so that the phase of the target response is close to other paths. When the phase difference between some of the transfer paths and the target response is reduced, their combined contribution is increased. The target response is increased when the combined contribution is increased beyond the reduced contribution amount. So, reducing the

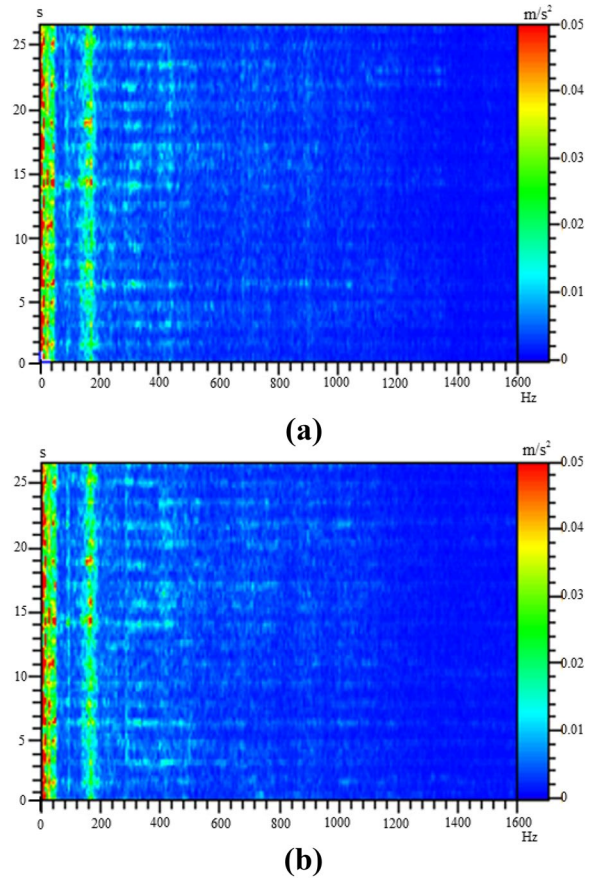

Figure 9 Comparison between **a** calculated and **b** measured values of the target point

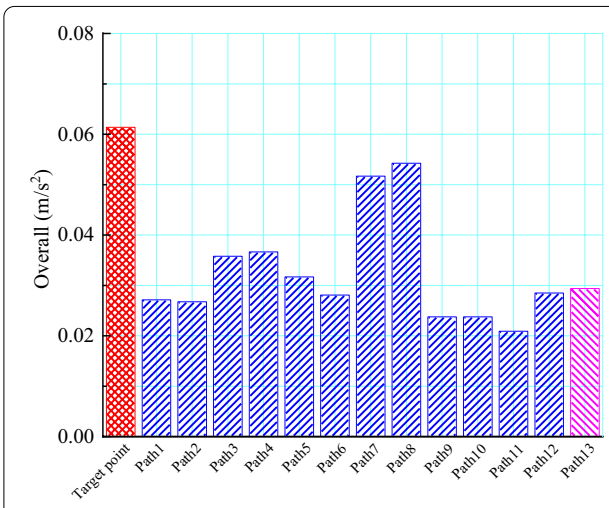

Figure 10 Overall value of the transfer paths' contributions; path definitions are listed in Table 3

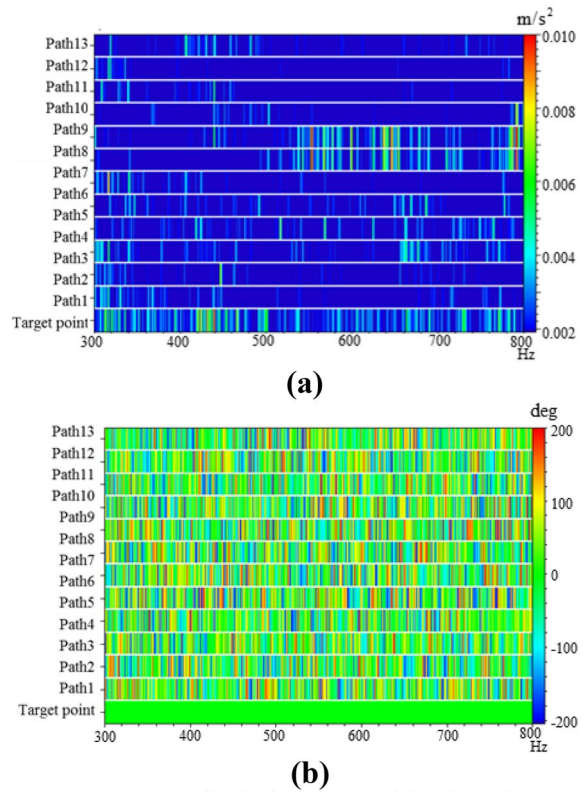

Figure 11 **a** Amplitude–frequency and **b** phase–frequency relationship

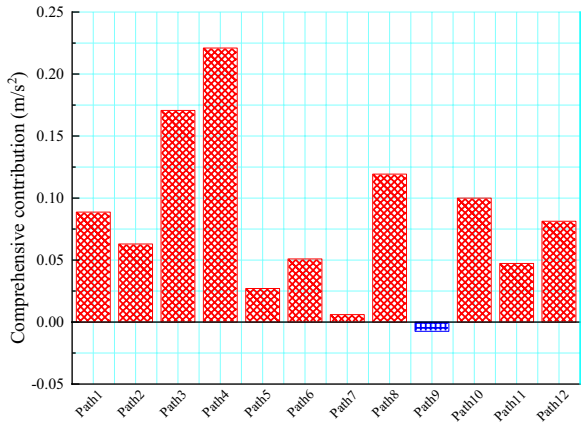

Figure 12 Contribution of secondary transfer paths over the range of 300–800 Hz

contribution of one transfer path too much is not conducive to the reduction of the target response. It can be seen from Figure 13 that the contributions of each transfer path changed when the two major transfer paths obtained by Method B were reduced to different degrees.

Table 4 Comparison of optimization methods

	Overall (10^{-2}·m/s^2)		Reduction ratio (%)	
	Method A	**Method B**	**Method A**	**Method B**
Initial	5.78	5.78	0	0
Reduce 20% 20%	5.70	5.43	1.38	6.06
Reduce 40% 40%	5.66	5.23	2.08	9.52
Reduce 60% 60%	5.69	5.19	1.56	10.21
Reduce 80% 80%	5.76	5.33	0.35	7.79

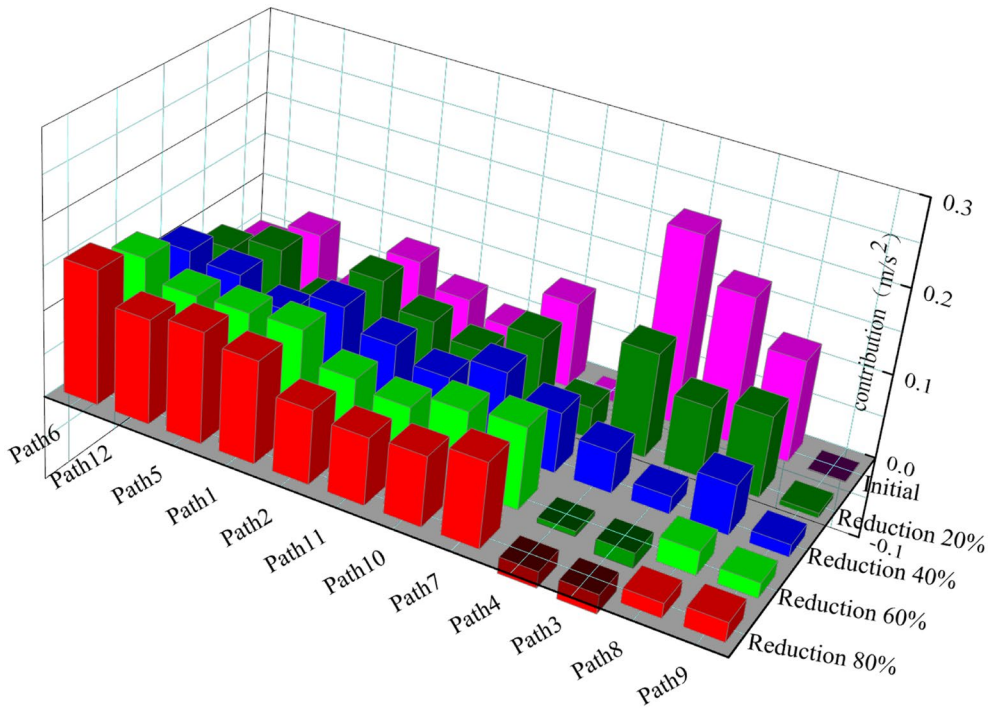

Figure 13 Change of contribution

Figure 13 shows that the contributions of other transfer paths may increase when that of the vertical direction of the anti-rolling torsion bar area and the longitudinal direction of the air spring area decreases, such as the vertical direction of the lateral damper area, the longitudinal and lateral direction of the anti-rolling torsion bar area, etc. Therefore, the overall value of the target point response increases when a path decreases too much. So, we cannot blindly optimize only the maximum transfer path when we want to reduce the response of the target point by optimizing transfer paths. While optimizing the maximum transfer path, we must also grasp the changes of other transfer paths to avoid excessive optimization resulting in no decrease in the target response.

This study proposes a series of optimization schemes in Table 5 to maximize the optimization benefit of the transfer paths and avoid over-optimization of a certain transfer path, assuming that once a transfer path is optimized, the contribution amplitude can be reduced by 10%, and the phase remains unchanged. A variety of optimization schemes are proposed, and the scheme number represents the number of optimizations; that is, Scheme 12 optimizes the transfer paths 12 times. The optimization rule selects the maximum transfer path according to the order of contribution obtained by Method B for optimization. The contribution order of the transfer paths is updated after each optimization, and the new maximum transfer path found is further optimized. For example, after the reduction according to Scheme 1, the maximum

Table 5 Optimization schemes

Number		1	2	3	4	5	6	7	8	9	10	11	12
Overall (m/s^2)		0.0568	0.0559	0.0551	0.0545	0.0539	0.0534	0.0529	0.0524	0.0519	0.0516	0.0511	0.0507
Reduction ratio (%)		1.8	3.3	4.7	5.8	6.8	7.6	8.6	9.4	10.1	10.8	11.6	12.3
Path and reduction ratio (%)	Path 1						10.0	10.0	10.0	10.0	10.0	10.0	10.0
	Path 3		10.0	10.0	19.0	19.0	19.0	19.0	19.0	27.1	27.1	27.1	27.1
	Path 4	10.0	10.0	19.0	19.0	27.1	27.1	27.1	27.1	27.1	27.1	34.4	34.4
	Path 6										10.0	10.0	10.0
	Path 10							10.0	10.0	10.0	10.0	10.0	19.0
	Path 12								10.0	10.0	10.0	10.0	10.0

path of the contribution is changed from the vertical direction of the anti-rolling torsion bar area to the longitudinal direction of the air spring area, so Scheme 2 is that the longitudinal direction of the air spring area's amplitude is reduced by 10%.

Table 5 shows the specific reduction paths, reduction ratios, corresponding target point response overall value, and overall value reduction ratios of the 12 optimization schemes according to the previous optimization rule. It can be observed that when the contribution of the vertical direction of the anti-rolling torsion bar area and the longitudinal direction of the air spring area are reduced by 27.1% and 19.0%, respectively, the vertical direction of the air spring area becomes the major transfer path, and the vertical and longitudinal directions of the core plate area and the longitudinal direction of the anti-rolling torsion bar area also become the maximum transfer path. It is possible to avoid the situation in which the target point response does not decrease after optimizing a certain path, and each optimization can reduce the target point response by adopting such an optimization method. Table 5 shows some optimization schemes, and more optimization schemes can be proposed to lower the overall value using this method. According to the desired overall value of the target point, the appropriate transfer path optimization scheme can be obtained through this table.

6 Conclusions

Based on the results described in this study, the following conclusions can be drawn:

(1) When the metro vehicles run on the roadbed section at speeds of 60 km/h, the dominant energy band of the interior noise is 300–800 Hz. According to the results of sound source identification, the significant sound source is located in the floor area, which is mainly caused by the vertical vibration of the floor. In the frequency range of 300–800 Hz, the main excitation of floor vertical vibration is structural excitation, accounting for 86.6%, with bogie area noise excitation accounting for 13.4%.

(2) The traditional OTPA contribution analysis method ignores the influence of the excitation phase. Based on the OTPA method, this study considered the influence of the excitation amplitude and phase, and analyzed the contribution of the secondary suspension path to the floor vibration when the metro vehicles were running on the roadbed section at speeds of 60 km/h. In the frequency range of 300–800 Hz, the vertical direction of the anti-rolling torsion bar area provided the maximum contribution to the floor vibration, with a contribution of 22.1%, followed by the longitudinal vibration of the air spring area, with a contribution of 17.1%.

(3) The transfer path optimization must be carried out step by step and multiple times. Each optimization scheme must be formulated based on the contributions of the previous optimization. In the optimized scheme of this study, when the contribution of the vertical direction of the anti-rolling torsion bar area and the longitudinal direction of the air spring area were reduced by 27.1% and 19.0%, respectively, the vertical direction of the air spring area became the major transfer path.

Acknowledgements
The authors sincerely thanks to Zhihui Li, Qi Wang, et al. (Southwest Jiaotong University) for their assistance in the measurements and data processing.

Authors' contributions
LP put forward the method, analyzed the data, and wrote the manuscript; JH, XX, and CM were in charge of the whole trial and reviewed the manuscript; JN assisted with measurements and data analyses. All authors read and approved the final manuscript.

Authors' Information
Laixian Peng, born in 1992, is currently a PhD candidate at *School of Mechanical Engineering, Southwest Jiaotong University, China*. He received his bachelor degree from *Southwest Jiaotong University, China*, in 2015. His research interests include railway noise and vibration.

Jian Han, born in 1987, is currently a postdoctor at *School of Mechanical Engineering, Southwest Jiaotong University, China*. He received his PhD degree from *Southwest Jiaotong University, China*, in 2018. His research interests include railway noise and vibration.
Jiaxing Nie, born in 1995, is currently an engineer at *Southwest Technology and Engineering Research Institute, China*. He received his Master's degree from *Southwest Jiaotong University, China*, in 2020. His research interests include railway noise and vibration.
Xinbiao Xiao, born in 1978, is currently an associate professor at *State Key Laboratory of Traction Power, Southwest Jiaotong University, China*. He received his PhD degree from *Southwest Jiaotong University, China*, in 2013. His research interests include railway noise and vibration.
Caiying Mi, born in 1965, is currently a professor at *School of Mechanical Engineering, Southwest Jiaotong University, China*. He received his PhD degree from *Southwest Jiaotong University, China*, in 2006. His research interests include optimization design of locomotive and rolling stock structure.

Funding
Supported by National Natural Science Foundation of China (Grant Nos. U1934203, U1734201), Sichuan Science and Technology Program(Grant No. 2020YJ0254) and Fundamental Research Funds for the State Key Laboratory of Traction Power (Grant No. 2019-Q02).

Competing Interests
The authors declare no competing financial interests.

Author Details
[1]School of Mechanical Engineering, Southwest Jiaotong University, Chengdu 610031, China. [2]Southwest Technology and Engineering Research Institute, Chongqing 400039, China. [3]State Key Laboratory of Traction Power, Southwest Jiaotong University, Chengdu 610031, China.

Received: 5 October 2020 Revised: 18 January 2022 Accepted: 18 February 2022
Published online: 29 March 2022

References

[1] D J Thompson. *Railway noise and vibration: mechanisms, modelling and means of control.* Amsterdam: Elsevier, 2009.
[2] D J Thompson. On the relationship between wheel and rail surface roughness and rolling noise. *Journal of Sound and Vibration*, 1996, 193: 149–160.
[3] R Fan, Z Su, G Meng, et al. Application of sound intensity and partial coherence to identify interior noise sources on the high speed train. *Mechanical Systems and Signal Processing*, 2014, 46: 481–493.
[4] J Zhang, X Xiao, X Sheng, et al. Sound source localisation for a high-speed train and its transfer path to interior noise. *Chinese Journal of Mechanical Engineering*, 2019, 32: 59.
[5] T Ahlersmeyer. Transfer path analysis – a review of 18 years of practical application. *International Conference on Acoustics*; Rotterdam: NAG-DAGA, 2009: 761–763.
[6] AS Elliott, AT Moorhouse., T Huntley, et al. In-situ source path contribution analysis of structure borne road noise. *Journal of Sound and Vibrations*, 2013, 332(24): 6276–6295.
[7] J Plunt. Finding and fixing vehicle NVH problems with transfer path analysis. *Sound and Vibration*, 2005, 39(11): 12–16.
[8] MV der Seijs, D de Klerk, DJ Rixen. General framework for transfer path analysis: History, theory and classification of techniques. *Mechanical Systems and Signal Processing*, 2016, 68–69: 217–244.
[9] A Grosso, M Lohrmann. Operational transfer path analysis: Interpretation and understanding of the measurement results using response modification analysis (RMA), *SAE Technical Paper* 2016-01-1823, 2016.
[10] D de Klerk, A Ossipov. Operational transfer path analysis: Theory, guidelines and tire noise application. *Mechanical Systems and Signal Processing*, 2010, 24(7): 1950–1962.
[11] G De Sitter, C Devriendt, P Guillaume, et al. Operational transfer path analysis. *Mechanical Systems and Signal Processing*, 2010, 24(2): 416–431.
[12] T Keizer, D de Klerk. Operational transfer path analysis applied to a ship with multiple engines, gearboxes and propellers. *EuroNoise 2015*, Maastricht, The Netherlands, 2015: 879–884.
[13] R. Ström. Operational transfer path analysis of components of a high-speed train bogie, Master's Thesis, Chalmers University of Technology, Göteborg, Sweden, 2014.
[14] P Gajdatsy, K Janssens, L Gielen, et al. Critical assessment of operational path analysis: Mathematical problems of transmissibility estimation. *The Journal of the Acoustical Society of America*, 2008, 123(5): 3869.
[15] J Putner, M Lohrmann, H Fastl. Contribution analysis of vehicle exterior noise with operational transfer path analysis. *Proceedings of Meetings on Acoustics*, 2014, 19: 040035.
[16] T Mihkel. Operational transfer path analysis: A study of source contribution predictions at low frequency, Master's Thesis, Chalmers University of Technology, Göteborg, Sweden, 2012.
[17] W Cheng, Y Chu, X Chen, et al. Operational transfer path analysis with crosstalk cancellation using independent component analysis. *Journal of Sound and Vibration*, 2020, 473: 115224.
[18] J Zhang. *Transfer path research of noise and vibration and its application*. Beijing: Beijing Jiaotong University, 2015. (in Chinese)
[19] P Lei. Study of transfer path analysis to interior noise source of subway vehicle. Beijing: Beijing Jiaotong University, 2016. (in Chinese)
[20] Hee-Min Noh. Contribution analysis of interior noise and floor vibration in high-speed trains by operational transfer path analysis. *Advances in Mechanical Engineering*, 2017, 9(8): 1–14.
[21] J Putner, H Fastl, M Lohrmann, et al. Operational transfer path analysis predicting contributions to the vehicle interior noise for different excitations from the same sound source. *41st International Congress and Exposition on Noise Control Engineering*, New York City, USA, August 19-22, 2012.
[22] M Lohrmann. Operational transfer path analysis: Comparison with conventional methods. *The Journal of the Acoustical Society of America*, 2008, 123(5): 3534.
[23] B Rafaely. Plane-wave decomposition of the sound field on a sphere by spherical convolution. *The Journal of the Acoustical Society of America*, 2004, 116(4): 2149–2157.
[24] Z Chu, Y Yang, Y He. Deconvolution for three-dimensional acoustic source identification based on spherical harmonics beamforming. *Journal of Sound and Vibration*, 2015, 344: 484–502.